Turkish Journal of Electrical Engineering & Computer Sciences

http://journals.tubitak.gov.tr/elektrik/

Research Article

Turk J Elec Eng & Comp Sci
(2016) 24: 5078 – 5089

doi:10.3906/elk-1504-189

Interference in geoelectric field observation from the current of a direct-current grounding electrode

Bo TANG, Zhuo WU*, Ren LIU, Shuang WANG, Qixiang LIN
College of Electrical Engineering and Renewable Energy, China Three Gorges University, Yichang, Hubei, P.R. China

Received: 22.04.2015 • **Accepted/Published Online:** 29.10.2015 • **Final Version:** 06.12.2016

Abstract: The existence of ultrahigh voltage direct-current (UHVDC) transmission lines impacts geoelectric field observation (GFO), which further disturbs earthquake observation and prediction. We proposed a mathematic method based on a 3-dimensional layered soil model to calculate the interference and conducted GFO experiments at observatories and field observation sites during the live debugging of a ±800 kV UHVDC transmission line to verify the method. The results obtained by using the proposed method are in good accordance with the experimental results and the maximum error is no more than 15%. Moreover, the experiment proves that grounding current is a decisive factor in the interference from a transmission line to GFO.

Key words: Ultrahigh voltage direct-current transmission line, geoelectric field observation interference, grounding current, 3-dimensional complex layered soil model, interference experiments of geoelectric field observation

1. Introduction

Using high voltage direct-current (HVDC) lines has many advantages in transmitting large-capacity power long distances and to set up power networks. They have become the key method in the construction of the smart grid in China [1,2]. However, the construction and operation of ultrahigh voltage direct-current (UHVDC) transmission lines will inevitably cause interference in observation devices in nearby earthquake observatories [3,4], which may disturb earthquake observation and prediction.

Earthquake observation is mainly composed of measurements of geomagnetic field, geoelectric field, and soil resistance [3], all of which could be interfered with by operating UHVDC transmission lines. The interference in geomagnetic observation from UHVDC lines has been studied rather well in China, as reported in [5–7], where calibration measurements were also proposed. However, there are only a few studies on the interference in geoelectric field observation (GFO) and soil resistivity measurement from UHVDC lines [8]. When the ±500 kV Baoji–Deyang DC line was operating in single-pole mode, the GFO in the Guanzhong area of China (mainly western parts of China) was found to be significantly interfered with [9]. Interference in GFO experiments was also reported when the ±800 kV Xiangjiaba–Shanghai UHVDC line was in live debugging [5]. In [10,11], these interferences from the compound electric field of polar conductors and grounding current were analyzed based on a theoretical method and, according to the results, it was hypothesized that grounding current was the decisive factor in the interference.

Based on the results reported in [10,11], according to the soil condition around the grounding electrode

*Correspondence: 364194605@qq.com

of the ±800 kV Jinping–Sunan UHVDC transmission line, we established a 3-dimensional (3D) layered soil model to calculate the interference to GFO from grounding current. The model and calculation were verified by GFO experiments conducted at observatories and field sites during the live debugging. The results allowed for a foundation for developing the software to calibrate the interference from DC transmission lines to GFO in earthquake observatories, which is similar to the software for calibrating geomagnetic field observation that we developed before [5].

2. Interference from DC transmission lines to geoelectric field observation

2.1. Geoelectric field observation

"Geoelectric field" refers to the electric field distributed on the Earth's lithosphere. It is induced by all kinds of nonartificial current systems interacting with the conducting lithosphere.

A ZD9A is a kind of device widely used in China for GFO [3]. Generally, a ZD9A has its electrodes buried 1.5 m deep, and it measures the geoelectric field once every minute with resolution up to 10 μV. The measured geoelectric field intensity is the average of a number of potential differences between electrodes that are acquired continuously. As shown in Figure 1, O is an electrode buried in the middle of the observation site, while E, S, W, and N are 4 electrodes buried in 4 directions around O; E_o is the average electric field intensity at O, i.e. geoelectric field intensity, and it is calculated from the potentials at the 4 electrodes, namely φ_E, φ_W, φ_S, and φ_N [12].

$$E_o = \sqrt{(\frac{\varphi_E - \varphi_W}{L_{EW}})^2 + (\frac{\varphi_S - \varphi_N}{L_{SN}})^2} \tag{1}$$

Here, E_o is in mV/km, and L_{EW} and L_{SN} are the distances between E–W and S–N electrode pairs, respectively.

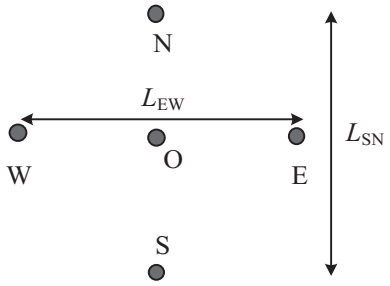

Figure 1. Electrode arrangement of geoelectric field observation instrument.

According to the standard [13] for GFO, the additional electric field intensity induced by artificial electromagnetic sources at frequencies other than power frequency shall be less than 0.5 mV/km.

2.2. Mechanism of interference to GFO from DC transmission lines

Geoelectric field intensity is normally obtained from potentials measured from buried electrodes [10,11]. The results in [10] indicated that interference from the current on polar conductors is negligible, whereas it is mainly grounding current that brings interference to GFO. The measured geoelectric field intensity comprises the actual geoelectric field and the electric field at the electrodes of measurement devices induced by grounding current, i.e. geoelectric field intensity is the observed value of geoelectric field measurement devices after subtracting the interference induced by grounding current.

3. Model for calculation of the potential in soil of grounding current

3.1. Mathematical model of soil

The potential of grounding current in soil can be obtained by using Green's function according to the soil model [14,15]. We used the equivalent complex image method to get Green's function at complex distances. This method not only simplifies the calculation but also has high computational accuracy [16].

For the UHVDC transmission lines in China, grounding electrodes are generally horizontally buried in concentric double-circle setups, as shown in Figure 2. Therefore, the soil model here is horizontally layered in the vertical direction, and it takes the grounding electrode and geoelectric field measurement electrodes in the same layer, i.e. both source points and field points are in the first soil layer. The first layer also needs to be vertically layered to fit the geological features of surface soil. Normally the distance between the grounding electrode and observation site is more than 1 km. Taking into account the excessive computational loads of solving 3D complex soil models [16,17], here we only vertically laminate the surface layer of a horizontally layered soil model in the direction from the source point to the observation site to obtain the complex soil model for calculating the potential of grounding current in soil, as shown in Figure 2.

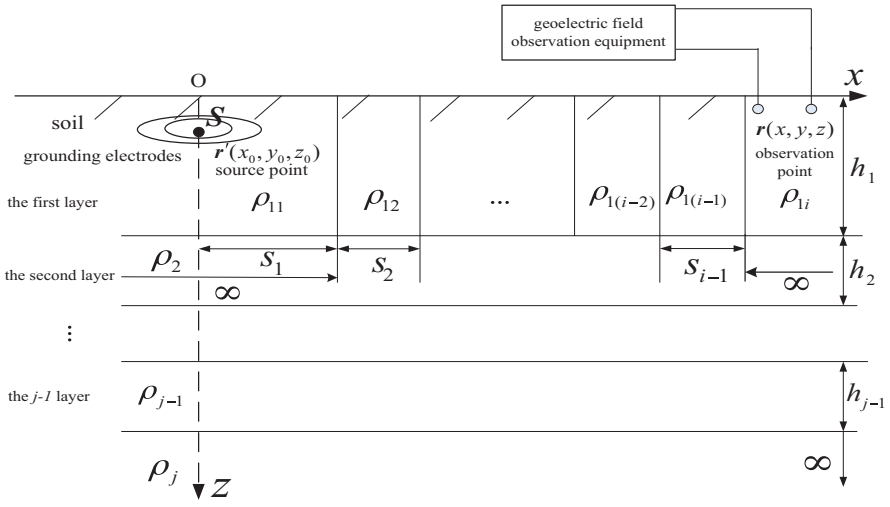

Figure 2. Complex soil model for calculating interference to geoelectric field observation from grounding current.

3.2. Potential calculation with complex soil model

As shown in Figure 2, the x-axis is from source point O to observation point, while the z-axis is vertically downward from the source point. There are n horizontal layers of the soil model along the $z-$axis, which have resistivity of ρ_{z1}, ρ_{z2}, ..., $\rho_{z(n-1)}$ and thicknesses of h_1, h_2, ..., $h_{(n-1)}$, h_n (where $h_n = \infty$). Meanwhile, the first layer is divided into n vertical layers, which have resistivity of ρ_{x1}, ρ_{x2}, ..., $\rho_{x(n-1)}$, ρ_{xn} and thickness of x_1, x_2, ..., x_{n-1}, x_n (where $x_1 = x_n = \infty$). The grounding current is taken as a point current source $\mathbf{r}'(x_0, y_0, z_0)$ located in block ρ_{x1}, and a random field point $\mathbf{r}(x, y, z)$ located in any block ρ_{xi} represents the measuring electrode of the GFO device.

In Section 3.1, it was mentioned that solving the soil potential requires deducing Green's function according to the soil model. When the first horizontal layer is uniform without any lamination and the source point and field point are both located in it, Green's function in a rectangular coordinate system for the soil

model would be [16]:

$$G_{z11}(x,y,z)=\frac{\rho_{x1}}{4\pi}[\frac{1}{r_0}+\sum_{i=1}^{m_z}a_{zi}(\sum_{j=1}^{n_z}\frac{k_{zj}}{r_{zij}}+\sum_{k=1}^{l_z}\frac{p_{zk}}{r_{zik}})], \tag{2}$$

where $r_0=[(x-x_0)^2+(y-y_0)^2+(z-z_0)^2]^{0.5}$; $r_0'=[(x-x_0)^2+(y-y_0)^2+(z+z_0)^2]^{0.5}$,

$$r_{zij}=[(x-x_0)^2+(y-y_0)^2+(z-c_{zj}-b_{zi})^2]^{0.5};\quad r_{zik}=[(x-x_0)^2+(y-y_0)^2+(z-c_{zk}+b_{zi})^2]^{0.5}.$$

r_0 is the distance between the source point and the field point. r_{zij} and r_{zik} are distances between image points and the field point. $c_{zi}+b_{zi}$ and $c_{zk}-b_{zi}$ are the image points' coordinates in the z-axis direction. $a_{zi}k_{zj}$ and $a_{zi}p_{zk}$ are image coefficients; $m_zn_z+m_zl_z$ is the total image number.

When the soil model is vertically layered only, the corresponding Green function in a rectangular coordinate system becomes:

$$G_{x11}(x,y,z)=\frac{\rho_{x1}}{4\pi}[\frac{1}{r_0}+\sum_{i=1}^{m_x}a_{xi}(\sum_{j=1}^{n_x}\frac{k_{xj}}{r_{xij}}+\sum_{k=1}^{l_x}\frac{p_{xk}}{r_{xik}})] \quad , \tag{3}$$

where the variables are defined the same as in Eq. (2).

For a vertically layered soil model applied in practical situations, the influence of the ground surface needs to be taken into consideration. In this case, a term representing the effect of the source point's image shall be added into Eq. (3), i.e. we substitute $-x_0$ for x_0 in Eq. (3).

According to Eq. (3), in a soil model layered vertically in the x-axis direction, the image points vary only in their x-coordinates and remain the same in their y-coordinates and z-coordinates. By setting several matched image points in the horizontal direction, which fulfills the boundary conditions of the vertical layers in a horizontal layer, this horizontal layer can be taken as uniform, with resistivity of ρ_{x1}. Likewise, we can also simplify multiple horizontal layers into one uniform layer by setting image points in the vertical direction. With all these image points in both directions, we can deduce a potential expression, i.e. Green's function, for the complex soil model shown in Figure 2.

$$\psi_{zx11}(x,y,z)=\frac{\rho_{x1}}{4\pi}\{G_{11}(z_0)+\sum_{i=1}^{m_z}a_{zi}[\sum_{j=1}^{n_z}k_{zj}G_{11}(x,y,z-c_{zj}-b_{zi})+\sum_{k=1}^{l_z}k_{zj}G_{11}(x,y,z-c_{zk}+b_{zi})]\} \tag{4}$$

Furthermore, if the source point and field point are distributed in different soil layers, by varying the positions and sizes of the image points in the model layers properly we can also obtain Green's function by taking all of these image points into account.

Figure 3. Relative position of experiment monitoring points and ±800 kV Jinping–Sunan UHVDC power line (from Google Maps).

4. Experimental study of the interference from UHVDC transmission lines to GFO

4.1. Experimental setup

On the Xiangjiaba–Shanghai UHVDC transmission line, one grounding electrode (30°49.662′N120°27.753′E24 m above sea level) is at the Tongli converter station, and the other (27°54.251′N, 102°36.416′E, 2668 m above sea level) is at the Yulong converter station. The locations of these sites are shown in Figure 3 and their geographic coordinates are listed in Table 1, where the distances are TopView values that were calculated based on global positioning system (GPS) coordinates.

Table 1. Coordinates of observed geoelectric field positions in the experiment.

Distance from power line (m)	Geoelectric observation position	Longitude (°)	Latitude (°)	Altitude (m)
85,246	Wuhan station	114.506	30.507	58
1368.72	In-field A	114.352	29.782	38
40,125	Xiaomiao station	102.220	27.910	1576
148,237	Nanjing station	119.017	31.317	30
116,107	Qingpu station	121.104	31.142	3
658.01	In-field B	120.469	30.825	2

In November 2012, the ±800 kV Jinping–Sunan UHVDC line started its full-voltage, full-power live debugging. During this period, we set up interference observation sites along the transmission line and conducted geoelectric field measurements using devices with resolution of 10 μV.

Note that there are two observation sites, namely the Wuhan Earthquake Observatory and field observation point A, at the middle part of the line. Both sites are more than 600 km away from the grounding electrodes. These two were chosen to minimize the interference from the grounding current, which helps to verify the interference from the complex electric field from the power line.

4.2. Observation of grounding current

During our GFO experiments, we recorded the current of the UHVDC system on 26 November 2012. The data were recorded in Beijing standard time to be in accordance with the GFO data.

During the debugging period, it was not possible to record the current automatically; instead it was obtained by analyzing manually captured screen images, which made it not time-continuous. In the duration from 08:04:16 to 21:02:57 on 26 November 2012, 379 data points of grounding current were recorded, as shown in Figure 4. The resolution of current data was 1 A.

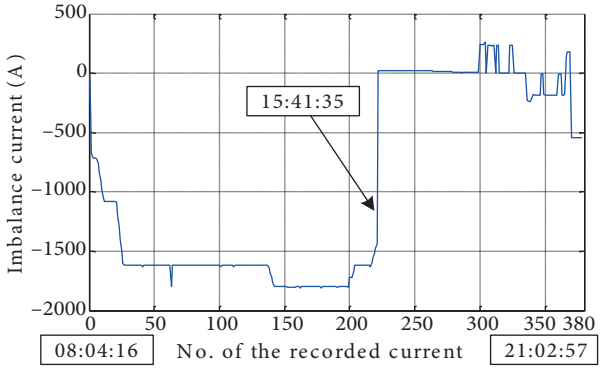

Figure 4. Measured grounding current on UHVDC power line.

5. Comparison between experiment and calculation

5.1. Soil model

As an example we took the grounding electrode at the Yulong converter station. The distance between the grounding electrode and the Xiaomiao Earthquake Observatory is 40,125 m, as measured by TopView. The landform of this area captured by Google Earth is shown in Figure 5.

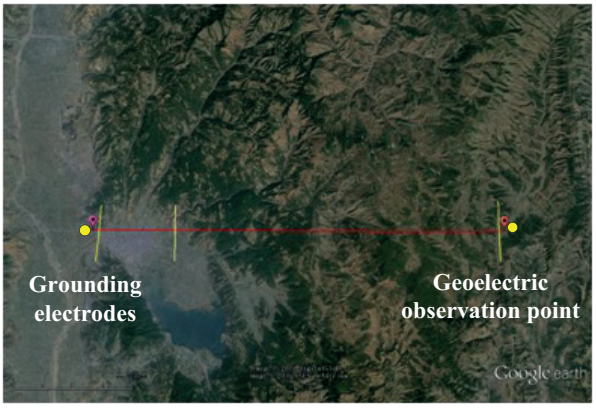

Figure 5. Landform between Yulong converter and Xiaomiao Earthquake Observatory (from Google Earth).

Using the mathematical model presented in Section 3.1, based on the soil features at the grounding electrode, the soil model is divided into 4 horizontal layers: the first layer has resistivity $\rho_{11} = 42.6\ \Omega.m$ and thickness $h_1 = 3$ m; the second layer has resistivity $\rho_2 = 572\ \Omega.m$ and thickness $h_2 = 10$ m; the third layer has resistivity $\rho_3 = 105\ \Omega.m$ and thickness $h_3 = 38$ m; and the fourth layer has resistivity $\rho_4 = 31\ \Omega.m$ and thickness $h_4 = \infty$.

The first layer is then vertically layered. The soil's resistivity around the grounding electrode and the observation site was measured manually. Since the TopView distance between the grounding electrode and the observation site is excessively long (over 40 km) and the landform is quite complex, it is hard to precisely determine the vertical layers according to the actual soil condition. As a result, the boundaries between vertical layers are defined roughly according to the surrounding geographic conditions (as shown in Figure 5).

Taking the computational load into consideration, the soil model has one layer between the pole and the site. The whole 3D soil model is shown in Figure 6, where $\rho_{x1} = 42.6\ \Omega.m \quad x_1 = \infty; \rho_{x2} = 35\ \Omega.m x_2 = 7.17\ km; \rho_{x3} = 530\ \Omega.m x_3 = 32.245\ km$; and $\rho_{x4} = 50\ \Omega.m x_4 = \infty$. In Figure 6, both the source point and the observation point have certain distances from the adjacent vertical boundaries.

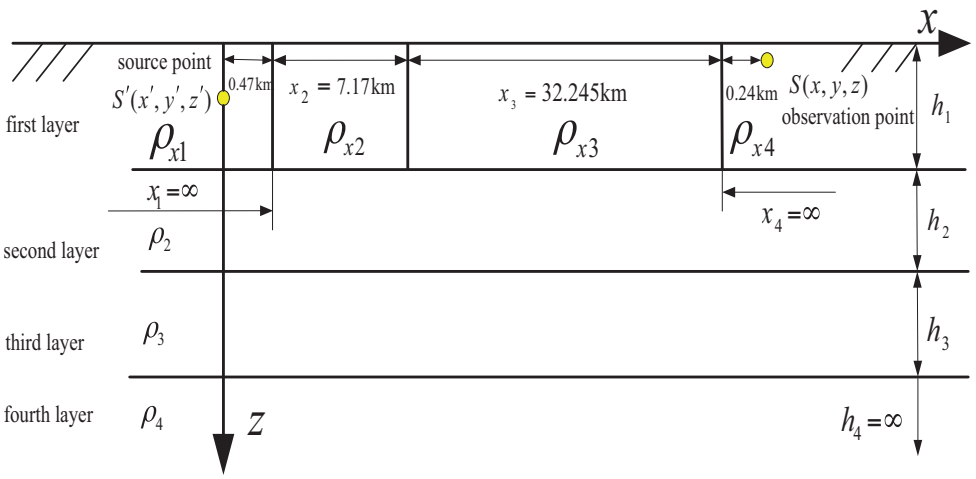

Figure 6. Soil model between Yulong converter and Xiaomiao Earthquake Observatory.

All the soil models between the other grounding electrodes and observation points used in this paper are established likewise. Using the method described in Section 3.1, the additional potential at observation points induced by grounding current are calculated. The interference electric field intensity is then calculated according to Eq. (1).

5.2. Comparison between experimental and calculation results

During the experiment, the Wuhan Earthquake Observatory and field observation point A were more than 600 km away from any grounding electrode, though the two observatories are relatively close to the power transmission line. The measurement results at these two sites were regular and showed no sign of interference, which suggests that the interference to GFO from polar conductors is negligible. However, the other observatories nearer the grounding electrodes were interfered with. This indicates that the grounding current is the decisive factor of the interference, which agrees with the hypothesis proposed in [10,11]. The measured electric field intensity and calculated interference intensity at Xiaomiao, Qingpu, In-field B, and Nanjing station were plotted as shown in Figure 7. In Figure 7, the figures on the left side are measured data using a ZD9A, and the figures on the right side are calculated data. For each site, the two figures have certain parts that overlapped in time. However, since the grounding current was recorded discontinuously, the figures' horizontal axes are not fully matched.

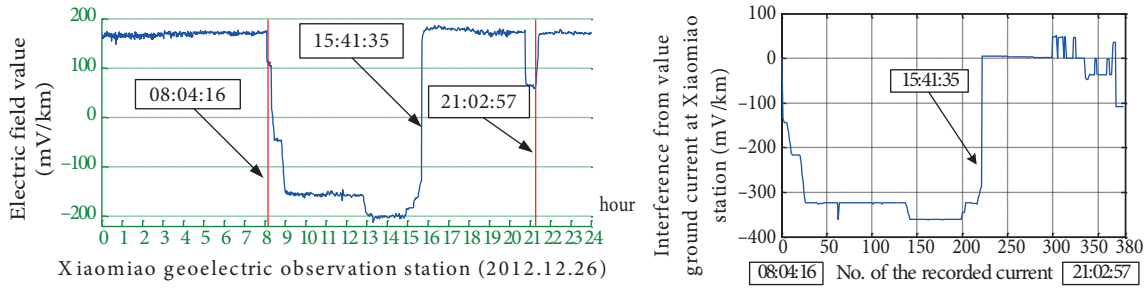

a. Xiaomiao earthquake observatory

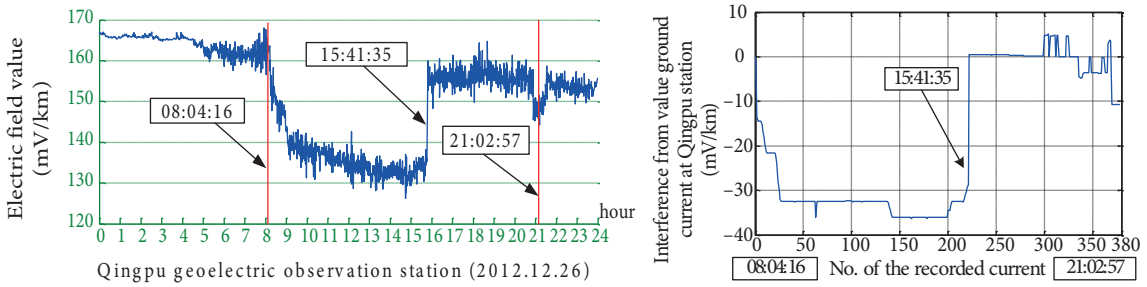

b. Qingpu earthquake observatory

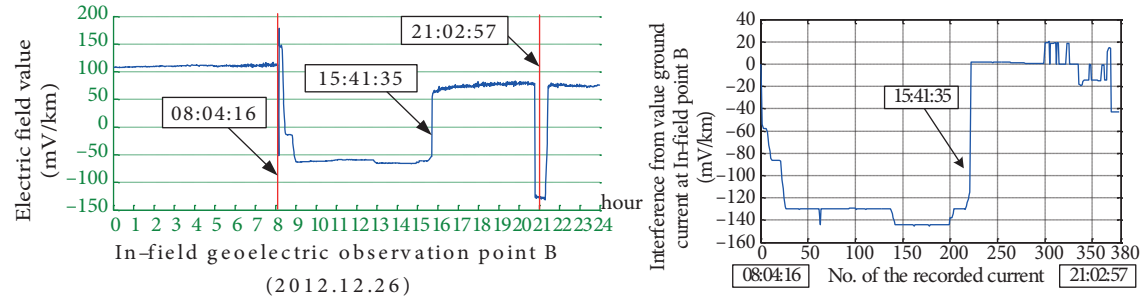

c. Field observation site B

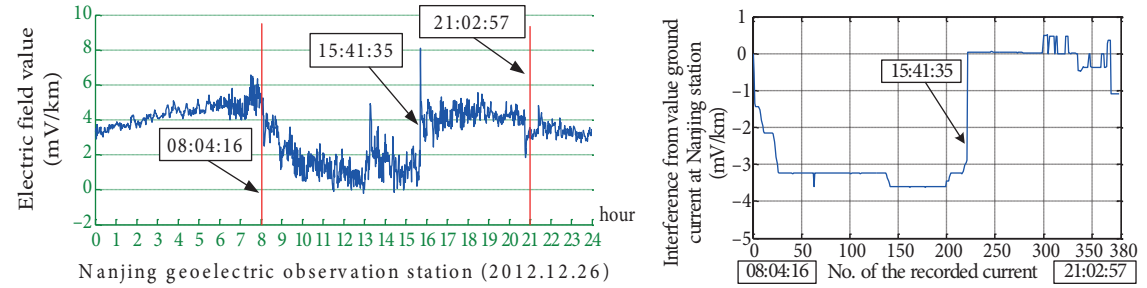

d. Nanjing earthquake observatory

Figure 7. Comparison between experimental and calculation results at four sites.

According to Figure 7, the geographic electric fields at the four sites varied in a similar pattern: all of them have cascade-like sharp variations that started at the same time. This clearly proves that the variations

were induced by external interferences. Figure 4 and Figure 7 show that the sudden change in geoelectric field intensity is similar to that of the grounding current. All the interference values have exactly the same form except for scaling in the y-axis, because the form was primarily determined by the grounding current, while the amplitude differed due to the different distances of each site from the grounding electrodes.

However, even without any interference, geoelectric field intensity has nonstationary variations [12], which are generally within 10 mV/km and are observed as burrs on the measured waveforms of geoelectric field intensity. Hence, when the grounding current is small and the observation point is far from the grounding electrode, the interference from the grounding current will be hard to distinguish from the self-variation of geoelectric field.

5.3. Error analysis

According to Section 5.1, the calculated geoelectric field interference is similar to the change in measured geoelectric field intensity: the two increased or decreased simultaneously though the variations of amplitudes were different. The error between measured and calculated data is listed in Table 2, where the error percentage is the increase in the observed value divided by the difference between the observed value and the calculated value.

Table 2. Interference in observed geoelectric field intensity.

Geoelectric observation position	Difference between calculation and measurement			Difference percentage (%)			
	Min (mV/km)	Max (mV/km)	Ave (mV/km)	Standard deviation	Min	Max	Average
Qingpu	0.05	2.63	1.01	0.8836	1.4327	15.6319	5.5914
Xiaomiao	0.28	2.12	1.23	0.7597	0.1240	14.5738	5.6597
In-field B	0.48	1.68	1.27	0.45	1.1136	11.5384	4.7009
Nanjing	0.05	0.99	0.38	0.43	1.1364	544.444	125.77

The reasons for these errors are briefly discussed as follows:

1. Modeling error: In the calculation model of interference in GFO caused by the DC grounding electrode, the annular grounding electrode was simplified into a point current source, and this brings a certain error. Besides, the soil model has many simplifications and it is only roughly layered due to the large dimensional scale (tens of kilometers) for calculation. This ideal process could result in a large difference from the resistivity distribution of actual soil, which also brings modeling error to the calculation results.

2. According to the calculations of various soil models, it is observed that resistivity of the soil near the grounding electrode (ρ_{x1} in Figure 6) has a relatively large influence on the calculation results. Hence, it is suggested that ρ_{x1} should be accurately acquired in practical applications.

3. Observation error: In the interference calculation, almost all the data were measured recently. The error in measurements directly impacts the calculation. Following Eq. (1), the resolution of the GFO device, 10 μV, turns out to be 0.25 mV/km in the calculated electric field intensity, i.e. the calculated results

could easily have an error of up to 0.25 mV/km due to measurement resolution. Likewise, the relatively low resolution of the grounding current record also brings errors to the calculation.

4. GPS locating precision: Currently, the precision of civilian GPS systems is tens of meters. Using these GPS systems in locating observation points may influence the accuracy of interference calculations.

5. In the experiments, data were acquired in units of several minutes. Since the geoelectric field is a continuous function in time, the measured acquired geoelectric field intensity variation comprises not only the interference from grounding current but also the geoelectric field's own nonstationary variation. Taking the recorded geoelectric field intensity at the Qingpu Earthquake Observatory at 12:00–13:00 on 28 November 2012 for example, the intensity waveform is plotted with a time interval of 1 min as shown in Figure 8.

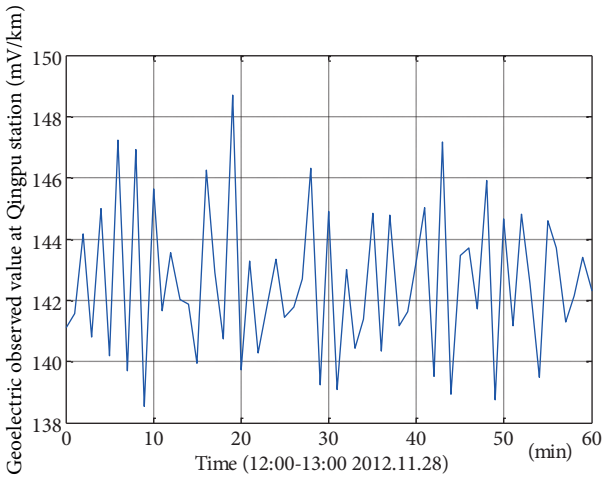

Figure 8. Geoelectric field intensity at Qingpu Earthquake Observatory.

From Figure 8, the geoelectric field changes each minute. The variation of amplitude is between 0.16 mV/km and 8.97 mV/km; the average is 3.712 mV/km. That is to say, for any interference in GFO smaller than 10 mV/km, the regular variation in geoelectric field could bring error of over 50% to the measured interference.

In this experiment, the interference observed at the Nanjing Earthquake Observatory is only several mV/km; it is mixed up with the geoelectric field's natural variation. The error analysis based on the data from Nanjing Earthquake Observatory was consequently lacking in accuracy and was neglected.

6. Conclusion

1. The observed geoelectric field data comes from ZD9A devices, and they are discrete as per minute. Therefore, it is difficult to accurately remove the interference from the perspective of signal analysis. Hence, with the proposed mathematical method, real-time computing of interference is achieved through the real-time values of grounding current and geoelectric field intensity, and this could be a reasonable way to realize real-time correction of GFO.

2. The experiment analysis suggests the interference calculated using the proposed method agrees with the experimental measurements well: the maximum error was no more than 15%. Plus, the experiments verified the hypothesis that the grounding current is the key factor determining the interference from transmission lines to GFO.

3. When the distance between the grounding electrode and observation site is hundreds of kilometers, the interference could be so small that it is equivalent to the normal variation of geoelectric field intensity, and the two will be hard to distinguish. On the other hand, the calculation results for smaller regions (tens of kilometers) are decent, with acceptable accuracy. Taking into account that the larger the target geographical region is, the harder it is to establish its precise soil model, the mathematical method proposed in this paper is suggested for calculating the interference in GFO at sites within a 100 km range from grounding poles of UHVDC transmission lines.

Acknowledgments

This work was supported in part by the National Natural Science Foundation of China (51307098) and the State Key Laboratory of Alternate Electric Power System with Renewable Energy Sources (LAPS14016).

References

[1] Liu ZY. Ultra-High Voltage Grid. Beijing, China: China Economy Press, 2006 (in Chinese).

[2] Zhao WJ. HVDC Engineering Technology. Beijing, China: China Electric Power Press, 2004 (in Chinese).

[3] Hu YX. Earthquake Engineering. Beijing, China: Earthquake Press, 2006 (in Chinese).

[4] Electric Power Research Institute of Energy Department. Experimental Research of Environmental Impact from 500 kV Power Line (Experimental Research on Seismic Station from Power Lines). Beijing, China: China Electric Power Research Institute, 1989 (in Chinese).

[5] Tang B, Zheng X, Zhang JG, Liu XF, Ge GZ. Interference from UHVDC power line on geomagnetic observation and its correction. IEEE T Power Deliver 2013; 28: 1111-1119.

[6] Qi L, Cui X, Wu Y. Minimum distance between AC transmission line and seismic observation station. High Voltage Engineering 2010; 36: 649-656.

[7] Tang B, Wen YF, Liu HZ, Zhang XW, De DQ, Fang FQ. Influence of DC transmission line on geomagnetic observation. High Voltage Engineering 2011; 37: 952-960.

[8] Shi HJ. Analysis on the interference factors in geoelectric field observation. Seismological Research of Northeast China 2009; 25: 51-57.

[9] Fang W, Zhang GQ, Shao HC. Study on the impact of HVDC to geoelectric field observation. Seismology and Geology 2010; 32: 434-441.

[10] Tang B, Zhang XW, Ge GZ, Zhang JG, Liu XF, Qu ZH. Interference on geoelectric field observation from UHVDC power line and its ground electrode. High Voltage Engineering 2013; 39: 2951-2959.

[11] Tang B, Ge GZ, Zhang JG, Liu XF, Huang Y. Interference from UHVDC power lines on geoelectric field observation with different electrode arrangements. East China Electric Power 2013; 41: 1653-1657.

[12] Monitoring and Prediction Department, China Earthquake Administration. Digital Observation Technology of Seismic Electromagnetic. Beijing, China: Earthquake Press, 2002 (in Chinese).

[13] Standardization Administration of China. Technical Requirement for the Observational Environment of Seismic Stations - Part 2: Electromagnetic Observation. Beijing, China: Standard Press of China, 2004 (in Chinese).

[14] Yuan JS, Li ZX. Complex image method for calculating electrostatic field in multilayer media. Journal of Tsinghua University (Science & Technology) 1999; 39: 51-53.

[15] Villas JET, Portela CM. Calculation of electric field and potential distributions into soil and air media for a ground electrode of a HVDC system. IEEE T Power Deliver 2003; 18: 867-873.

[16] Pang ZH, Zhang L, Tan B, Wen XS. Green's function of vertical multi-layer soil. Proceedings of the CSEE 2011; 31: 150-156.

[17] Sun JZ, Liu L. Derivation of Green's function by equivalent complex image method in a horizontal and vertical combined-layer soil structure. Proceedings of the CSEE 2003; 23: 146-151.